Phase Contrast at Ultra-High Field - Establishing the Imaging Workflow

Johannes Lindemeyer[1], Michael S. Poole[1], Desmond H. Y. Tse[1], Ana-Maria Oros-Peusquens[1], and N. Jon Shah[1,2]
[1]*INM - 4, Research Centre Jülich GmbH, Jülich, Germany,* [2]*Department of Neurology, RWTH Aachen University, Aachen, Germany*

Target Audience: Scientists with research interests in phase and susceptibility imaging or ultra-high field MRI

Purpose: Cerebral structures exhibit remarkably strong phase contrast at ultra-high field[1,2]. Nevertheless, the wave length used for imaging at 9.4T is on the order of 10^{-1}m within tissue, causing interference effects. Signal voids are induced by destructive interference of the transmit fields. The phase of the measured signal is caused by local and non-local B_0 variations and by chemical shift differences, but also by transmit RF phase variations and receive RF phase variations. Careful recombination of multiple receive channel data is necessary to avoid increasing noise in the phase maps (e.g. Robertson et al.[3]). The presented method attempts to recover the true phase evolution that takes place between excitation and acquisition. Only in this way can consistent phase images be established with the aim of fieldmap estimation and susceptibility reconstruction.

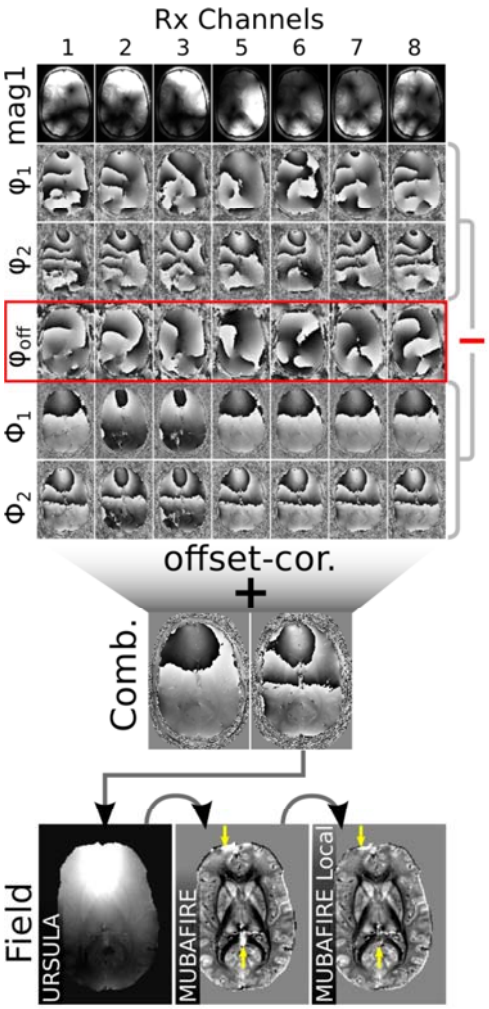

Figure 1: Processing scheme for multichannel phase data. The first and second echo are shown for the phase data.

Methods: Data were acquired with informed consent from a 26 year old male volunteer in a 9.4T human scanner (Siemens Healthcare, Erlangen, Germany) using an eight-channel Tx/Rx coil. The parametrisation included TR=33ms, TE=[4.65, 10.45, 16.25, 22.05] ms, $\alpha = 20°$ and a matrix size of $216 \times 256 \times 160$ voxels at 1mm isotropic resolution. The phase profile observed by a single channel can be described by the following model: $\varphi(\vec{r},t) = \varphi_0(\vec{r}) + \varphi_c(\vec{r}) + \Phi(\vec{r},t)$, where $\varphi_0(\vec{r})$ is the phase offset at excitation time, $\varphi_c(\vec{r})$ is the phase offset originating in the receive profile of channel c and $\Phi(\vec{r},t)$ is the true underlying phase evolution at position $\vec{r}$ and time t. Both phase offsets can be summarised by a channel-dependent offset phase, $\varphi_{off,c}(\vec{r}) = \varphi_0(\vec{r}) + \varphi_c(\vec{r})$. In order to estimate this offset, the field value, $b(\vec{r})$, is determined for each voxel and used to extrapolate the phase evolution to $t = 0$: $\varphi_{off,c}(\vec{r}) = \frac{1}{n}\sum_{i=1}^{n} \varphi(\vec{r},t) - t_i \cdot \gamma b(\vec{r})$, where n is the number of echoes recorded and t_i are the echo timings. The extrapolation operation, performed for each individual channel, includes averaging over all echo times. A comparable technique was also introduced by Robertson et al[3]. Yet, the estimation of the field, $b(\vec{r})$, is cumbersome, as ultra-high field phase data typically exhibit numerous phase poles (at the points in space where destructive interference of the RF fields occurs), rendering spatial unwrapping of the individual channels impossible (see Figure 1). Hence, the field for extrapolation is determined by unwrapping the echo differences, $\varphi(\vec{r},t_3) - \varphi(\vec{r},t_1)$ and $\varphi(\vec{r},t_4) - \varphi(\vec{r},t_2)$. This is applicable, since the phase poles are in $\varphi_0(\vec{r})$ and $\varphi_c(\vec{r})$, which are the same for each echo and thus vanish in the phase difference. Prelude[4] is employed for phase difference unwrapping. The phase offsets are actually determined for resampled datasets at half of the native resolution, to reduce the computational time. They are then interpolated to the native resolution and applied to the recorded data, yielding the true phase, $\Phi(\vec{r},t)$ for each channel. Resampling and interpolation are performed in complex representation. The offset-corrected data are combined by smoothed-magnitude-weighted complex averaging and the fieldmap at native resolution is determined employing once again Prelude for unwrapping. Background fields originating in external sources are identified and removed by MUBAFIRE (MUltistage BAckground FIeld REmoval, introduced by Lindemeyer et al.[5,6]). The MUBAFIRE Local extension then excludes field outliers by thresholding and compensates for their influences on the surroundings. Susceptibility reconstruction is finally performed using the minimization approach introduced by de Rochefort et al.[7] with hybrid Tikhonov- and gradient-regularisation (λ=0.06, mu=0.002, 25 iterations).

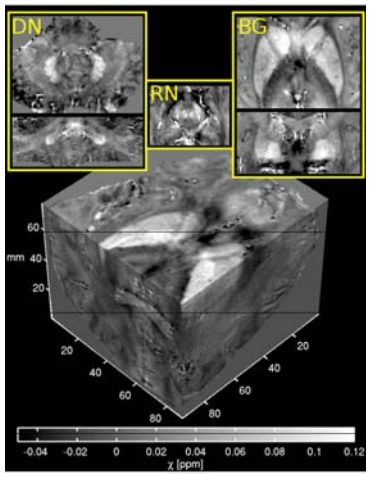

Figure 2: Susceptibility in orthogonal slices and zoomed view of dentate nuclei (DN), red nuclei (RN) and basal ganglia (BG)

Results: During multichannel recombination, one channel had to be excluded due to an abnormally high noise level. The recombination scheme is illustrated in Figure 1. The estimated true phase, $\Phi(\vec{r},t)$, for the channels 2 and 3 shows a constant offset with respect to the other channels which is removed before complex averaging. The recombined phase data contain no pronounced poles, but clean phase wrap surfaces as expected. The estimated fieldmap exhibits smooth characteristics and the background correction successfully removes external field perturbations. The corrected field as well as the susceptibility (see Figure 2) shows a high level of contrast. Figure 3 illustrates an exemplary zoomed view of cerebral gyri.

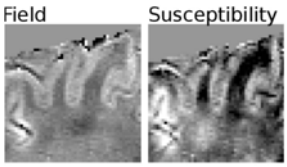

Figure 3: Field (left) and susceptibility (right) of cortical gyri

Discussion: Figure 1 indicates, that offset-sensitive correction is necessary for multichannel recombination at 9.4T. The presented processing chain allows for estimation of robust field and susceptibility maps, excluding external disturbances and pronouncing local tissue contrast (as shown in Figure 2). Interestingly, the contrast in the cerebral gyri is not increased by susceptibility reconstruction, but even slightly blurred. This effect might originate in blood vessels, disturbing reconstruction by their stray fields. It also might indicate other factors than susceptibility, e.g. chemical shifts, imparting an influence on the phase. In order to further improve the results, we will use parallel transmit techniques to ensure reliable phase measurement everywhere either by multiple acquisition with different transmitter phase settings for which the flip angle is spatially complementary, or by using kt-points or spokes excitation.

Conclusion: The presented processing chain enables phase, field and susceptibility mapping at 9.4T. Whilst generating excellent results for the moderate resolution used within this study, the approach serves as an ideal prerequisite for high-resolution phase imaging at ultra-high fields. Other sources of phase contrast, such as chemical shifts, should apparently be considered for studies at this field strength.

References:

1. Duyn, J. H. et al., High-field MRI of brain cortical substructure based on signal phase. PNAS. 2007, 104(28), 11796–801; **2.** Schäfer, A. et al., Direct Visualization of the Subthalamic Nucleus and its Iron Distribution Using High-Resolution Susceptibility Mapping. Hum Brain Mapp. 2012, 33(12), 2831–42; **3.** Robinson, S. et al., Combining Phase Images from Multi-Channel RF Coils Using 3D Phase Offset Maps Derived From a Dual-Echo Scan. Magnet Reson Med. 2011, 65: 1638–1648; **4.** Jenkinson, M.. Fast, Automated, N-Dimensional Phase-Unwrapping Algorithm. Magnet Reson Med. 2003, 49(1), 193–7; **5.** Lindemeyer, J. et al., Stepwise Filtering of Background Fields: Optimising Susceptibility Reconstruction. Proc of ESMRMB. 2011, p. 507, doi:10.1007/s10334-011-0268-5; **6.** Lindemeyer, J. et al., Microstructure Phase Imaging at 9.4T of the Human Brain Applying Stepwise Filtering of Background Fields. Proc Intl Soc Mag Reson Med. 2012, Vol. 20, 2329; **7.** De Rochefort, L. et al., Quantitative Susceptibility Map Reconstruction from MR Phase Data Using Bayesian Regularization: Validation and Application to Brain Imaging. Magnet Reson Med. 2010, 63(1), 194–206